

# Sound energy decay in coupled spaces using a parametric analytical solution of a diffusion equation

Paul Luizard<sup>a)</sup> and Jean-Dominique Polack

*Sorbonne Universités, UPMC Univ Paris 06, CNRS, UMR 7190, Institut d'Alembert, F-75005, Paris, France*

Brian F. G. Katz

*LIMSI-CNRS, BP133, F91403 Orsay, France*

(Received 1 July 2013; revised 13 January 2014; accepted 27 March 2014)

Sound field behavior in performance spaces is a complex phenomenon. Issues regarding coupled spaces present additional concerns due to sound energy exchanges. Coupled volume concert halls have been of increasing interest in recent decades because this architectural principle offers the possibility to modify the hall's acoustical environment in a passive way by modifying the coupling area. Under specific conditions, the use of coupled reverberation chambers can provide non-exponential sound energy decay in the main room, resulting in both high clarity and long reverberation which are antagonistic parameters in a single volume room. Previous studies have proposed various sound energy decay models based on statistical acoustics and diffusion theory. Statistical acoustics assumes a perfectly uniform sound field within a given room whereas measurements show an attenuation of energy with increasing source-receiver distance. While previously proposed models based on diffusion theory use numerical solvers, the present study proposes a heuristic model of sound energy behavior based on an analytical solution of the commonly used diffusion equation and physically justified approximations. This model is validated by means of comparisons to scale model measurements and numerical geometrical acoustics simulations, both applied to the same simple concert hall geometry.

© 2014 Acoustical Society of America. [<http://dx.doi.org/10.1121/1.4870706>]

PACS number(s): 43.55.Br, 43.55.Fw [JES]

Pages: 2765–2776

## I. INTRODUCTION

Prediction of sound field behavior in coupled volumes is of interest since this architectural feature is often met in everyday life: Large corridors linking smaller rooms, various connected rooms in factories, naves and side galleries in churches, stage houses in theaters, concert halls with acoustic reverberation or control chambers. These situations raise different issues concerning acoustics, from noise control to speech and music quality, depending on the function of the space. In each case a fine knowledge of sound field behavior is required for adapting the acoustical design to the functions of the venue. Therefore, prediction tools adapted to coupled volumes are necessary and various methods have been developed leading to more or less accurate results.

Among the available means for predicting the sound field behavior in coupled volumes one can use numerical methods based on geometrical or wave approaches, scale model measurements, or analytical expressions, each offering various levels of detail. This paper presents a theoretical model based on statistical acoustics and diffusion theory, with experimental validation through scale model measurements and comparisons made relative to simulations using geometrical acoustics software.

## A. Previous research

Among previous studies, two main model types are commonly used to describe sound energy decay in closed coupled spaces.

Statistical models are based on the diffuse sound field hypothesis developed by Sabine.<sup>1</sup> Pioneering studies by Davis<sup>2</sup> and Eyring<sup>3</sup> have proposed analytical models which describe the sound energy decay in a system of two coupled rooms. These results have been generalized for  $N$  coupled rooms and refined successively.<sup>4–8</sup> A model of energy density with spatial dependence without temporal component in the context of coupled rooms was introduced by Summers *et al.*<sup>8</sup> based on Barron's Revised Theory.<sup>9</sup> More recently, Summers<sup>10</sup> proposed another statistical model, accounting for time delay of energy transfer between coupled rooms, which tends to include a spatial component in the statistical model through consideration of travel time between rooms. Furthermore, a model describing sound energy decay in churches has been proposed by Martellotta,<sup>11</sup> using a sum of decaying exponential functions whose arguments are both time and space. Finally, a similar model combining spatial and temporal statistical decays in coupled volume concert halls with reverberation chambers has been recently presented.<sup>12</sup>

Diffusion theory was introduced in room acoustics by Ollendorff<sup>13</sup> and later continued by Picaut *et al.*<sup>14</sup> based on the idea that sound particles behave as fluid particles which collide into scattering objects within a propagation medium.<sup>15</sup> A recent study<sup>16</sup> derived the diffusion equation for room acoustics from a radiative transfer model, borrowed

---

<sup>a)</sup> Author to whom correspondence should be addressed. Also at: LIMSI-CNRS, BP133, F91403 Orsay, France. Electronic mail: paul.luizard@limsi.fr

from optics. This model can be developed under the assumption that spatial and temporal scales relative to the investigated acoustic phenomena allow for considering diffusion on boundaries as continuous and non-localized. Hence, this phenomenon is similar to diffusion within the entire volume. Another model based on the diffusion equation has been developed for single rooms in the case of cubic-like, long, or flat spaces.<sup>17</sup> Each approach propose a solution to the diffusion partial differential equation. Sound field modeling in coupled rooms with the diffusion equation has been proposed<sup>18</sup> with various absorption conditions,<sup>19,20</sup> coupling through partition walls,<sup>21</sup> and compared to scale model measurements.<sup>22</sup> A recent paper<sup>23</sup> investigated the effect of aperture size and receiver position in coupled spaces, which are both used in the present paper as means of validation of the proposed analytical model. Contrary to the present study, these studies<sup>17,19,21-23</sup> considered separate equations to describe sound behavior in the considered domain and on its surface; results were obtained using numerical solvers: Most of these studies used finite element software and the use of finite difference schemes has been introduced recently.<sup>24</sup>

## B. The present study

The present study proposes a heuristic model of sound energy variation based on a parametric analytical solution of the diffusion equation for single volume rooms and a hybrid numerical implementation for coupled volume rooms. This approach allows for a simple and fast representation of sound fields in single or coupled volume rooms. The proposed model estimates spatial sound energy decay in rooms based on source-receiver distance in steady state conditions and this sound energy level can then be considered as the initial level of temporal sound energy decay at each receiving position. Furthermore, the proposed analytical solution and its implementation require only one expression since the boundary conditions are embodied in a spatial diffusion term and a temporal damping term. As a consequence, simple calculation means can be used and performed in reduced time. Finally, this model is validated through comparisons with scale model measurements and numerical geometric methods, namely ray-tracing simulations, for various source-receiver arrangements and coupling area conditions. Results match those presented in a previous study<sup>23</sup> and additional configurations are tested, leading to new considerations on sound field in coupled spaces.

This paper is organized as follows: Section II presents the proposed analytical model based on the diffusion equation as well as the implementation adapted to coupled spaces. Section III describes the acoustical parameters used to quantify coupled impulse responses. Section IV presents the comparisons performed between the proposed model, measurements in a scale model, and ray-tracing simulations regarding two different issues: Distance variation between source, receiver, and coupling area, as well as coupling area variation. Section V is a general discussion of the results and Sec. VI concludes the paper.

## II. PROPOSED MODEL

The proposed model is derived from the diffusion equation adapted to room acoustics. This theoretical context is

based on the hypothesis of uniform distribution of scattering by objects within the volume under study, namely the walls of the room, which are supposed to be diffusely reflecting. This is a parametric model of energy density  $w(\mathbf{r}, t)$  which can be adapted to a large variety of room morphologies, absorption conditions, and source-receiver arrangements.

### A. Diffusion equation

The diffusion equation adapted to room acoustics describes energy flow from higher to lower density areas and can be written as follows:<sup>14,17</sup>

$$\frac{\partial}{\partial t} w(\mathbf{r}, t) - D \nabla^2 w(\mathbf{r}, t) + \sigma w(\mathbf{r}, t) = F(\mathbf{r}, t), \quad (1)$$

where  $D$  is the diffusion coefficient, linked to the spatial variation term, and the coefficient  $\sigma$  is related to the mean absorption  $\bar{\alpha}$  as shown in Eq. (3). Introducing the mean free path between two collisions  $\lambda = 4V/S$  makes it possible to express coefficients  $D$  and  $\sigma$  which are related to the room volume and total surface area.  $F(\mathbf{r}, t)$  is an arbitrary acoustic source term

$$D = \frac{\lambda c}{3} = \frac{4Vc}{3S}, \quad (2)$$

$$\sigma = \frac{c\bar{\alpha}}{\lambda} = \frac{c\bar{\alpha}S}{4V}. \quad (3)$$

Previous studies have shown that the absorption term  $\sigma$  can take alternative expressions that lead to more accurate results, especially for high boundary absorption. These expressions are obtained for example by replacing the Sabine absorption coefficient by the Eyring coefficient<sup>19</sup> or by a recently proposed alternative coefficient<sup>20</sup> reported as being more accurate for high global absorption conditions. Using such mean absorption coefficients might be less precise than when using distributed absorption within a numerical resolution of the diffusion equation.

### B. Proposed solution

The proposed model of spatial and temporal sound energy decay can be written as Eq. (4), inspired by the steady-state solution of the diffusion equation derived in a two-dimensional case<sup>14</sup>

$$w(\mathbf{r}, t) = \left( \frac{a}{r} e^{-\varepsilon r} + b \right) e^{-\gamma t} H\left(t - \frac{r}{c}\right), \quad (4)$$

where  $r = \|\mathbf{r} - \mathbf{r}_s\|$  is the source-receiver distance,  $\varepsilon$  is the spatial decay constant,  $\gamma$  is the temporal decay constant relative to sound absorption,  $c$  is the speed of sound, and  $a$  and  $b$  are positive real constant numbers to be adapted to each situation. The ratio  $a/b$  expresses the importance of the spatial decay as compared to the purely temporal statistical decay and can be referred to as the diffuse-to-statistical ratio. This point will be discussed in Sec. II C. For  $t < (r/c)$ , the sound energy density has its maximum value such that  $w(\mathbf{r}, t) = w(\mathbf{r})$  corresponding to a steady state excitation. Function  $H$  is the Heaviside step

function, standing for the fact that sound propagation requires a certain time to cover the source-receiver distance and reach the receiver position. Therefore, the temporal energy decay begins for each receiver with a time delay  $\Delta t = (r/c)$  after the cutoff of sound emission.

Furthermore, in classical statistical theory, as no spatial variation is considered, the power density balance equation is equivalent to the diffusion equation without the Laplacian term, as written in Eq. (5) for a steady state cutoff excitation. The solution of such an ordinary differential equation is a simple decaying exponential as in Eq. (6)

$$\frac{\partial}{\partial t} w(t) + \sigma w(t) = 0, \quad (5)$$

$$w(t) = w_0 e^{-\sigma t}. \quad (6)$$

This simple relation between diffusion and classical statistical theories shows that the absorption term is the same in both cases which means that  $\gamma = \sigma$ . Hence, the diffusion equation can be considered as a higher order statistical model of sound field behavior in an enclosure, accounting for spatial energy variation.

Considering steady state conditions, the energy density no longer depends on time. If the sound source is considered as a point source, then the source term can be written as the product of the source power and a spatial delta Dirac function  $F(\mathbf{r}, t) = P(t)\delta(\mathbf{r})$ . Thus, the stationary diffusion equation becomes Eq. (7) and the proposed energy density can be expressed as in Eq. (8)

$$-D\nabla^2 w(\mathbf{r}) + \sigma w(\mathbf{r}) = P\delta(\mathbf{r}), \quad (7)$$

$$w(\mathbf{r}) = \frac{a}{r} e^{-\varepsilon r} + b. \quad (8)$$

The Laplace operator in spherical coordinates applied to steady state energy density is expressed as Eq. (9)

$$\nabla^2 w(\mathbf{r}) = \frac{1}{r^2} \frac{d}{dr} \left( r^2 \frac{d}{dr} w(r) \right) = \varepsilon^2 \frac{a}{r} e^{-\varepsilon r}. \quad (9)$$

Equation (7) can then be integrated over a sphere, whose radius is the mean distance between the source and the walls, centered on the sound source using Ostrogradsky's theorem in spherical coordinates such that  $dV = dr^3 = r^2 \sin\theta dr d\theta d\phi$ . As a result, the first and second terms of Eq. (7) become Eqs. (10) and (11)

$$\int_V \nabla^2 w(r) dV = -4\pi a(1 + \varepsilon r) e^{-\varepsilon r}, \quad (10)$$

$$\int_V w(r) dV = \int_V a r e^{-\varepsilon r} dr \sin\theta d\theta d\phi + bV. \quad (11)$$

Thus, integrating of the whole Eq. (7) leads to

$$4\pi a \left( \frac{\sigma}{\varepsilon^2} + (1 + \varepsilon r) e^{-\varepsilon r} \left( D - \frac{\sigma}{\varepsilon^2} \right) \right) + \sigma bV = P, \quad (12)$$

which is verified for specific values of parameters  $\varepsilon$ ,  $a$ , and  $b$ . In fact, the quantity  $D - (\sigma/\varepsilon^2)$  must vanish so that the

exponential term disappears when  $r \rightarrow \infty$ , which leads to  $\varepsilon^2 = (\sigma/D)$  and  $4\pi a(\sigma/\varepsilon^2) + \sigma bV = P$ . The spatial decay parameter  $\varepsilon$  is then expressed in terms of the absorption and diffusion coefficients, and a theoretical relation is given between the magnitude parameters  $a$  and  $b$ . The first term of this equation does not account directly for the room's surface and volume because parameters  $a$  and  $b$  are empirically estimated.

Hence, the diffusion model proposed here can be written as Eq. (13), depending on the diffusion and absorption coefficients defined in Eqs. (2) and (3)

$$w(\mathbf{r}, t) = \left( \frac{a}{r} \exp\left(-\sqrt{\frac{\sigma}{D}} r\right) + b \right) \exp(-\sigma t) H\left(t - \frac{r}{c}\right). \quad (13)$$

## C. Asymptotic cases

### 1. Near field case

The proposed model is a sum of two terms whose relative weights are given by parameters  $a$  and  $b$ . As previously mentioned, these parameters represent the spatially dependent term and the Sabine term, respectively. Previous studies have proposed analytical models for which the sound energy density depends on space, particularly the source-receiver distance.<sup>9</sup> Measurements in concert halls,<sup>25</sup> churches,<sup>26</sup> and scale models<sup>27</sup> have confirmed that sound field energy density decays with increasing distance from the sound source. This phenomenon is particularly observable within a radius such that  $(a/r)\exp(-\sqrt{(\sigma/D)r}) \gg b$ . Within this perimeter where  $r$  is relatively small, the term governed by parameter  $a$  is predominant and the sound energy density can be approximated as

$$w(\mathbf{r}, t) \sim \frac{a}{r} \exp\left(-\sqrt{\frac{\sigma}{D}} r\right) \exp(-\sigma t) H\left(t - \frac{r}{c}\right). \quad (14)$$

### 2. Far field case

In special cases, the diffuse sound field hypothesis can be asymptotically met, typically requiring highly reverberant environments where absorption is very low,<sup>1</sup> such as reverberant chambers built to measure material absorption characteristics or some churches.<sup>28</sup> The application domain can be extended to various venues considering only the late part of the sound energy decay and large source-receiver distances, i.e., assuming the condition  $b \gg (a/r)\exp(-\sqrt{(\sigma/D)r})$ . The proposed model becomes Eq. (15) for which the spatial component only appears through the delay term, making it the only difference relative to the traditional Sabine sound decay model

$$w(\mathbf{r}, t) \sim b \exp(-\sigma t) H\left(t - \frac{r}{c}\right). \quad (15)$$

## D. Implementation and configuration for coupled spaces

The intention of this numerical implementation is to use the proposed model in combination with the classical

statistical theory. Initial energy levels are estimated in each room for steady state excitation conditions and temporal decays are further calculated at each receiver position. Acoustical coupling is taken into account through the initial sound level of each slope within the curved decay, estimated with respect to the coupling factor from statistical theory. Calculation of sound decay is performed in several steps.

- (1) Estimation of uniform sound energy density in each room with respect to the approach proposed by Cremer *et al.*,<sup>5</sup> governed by parameter  $b$  of the proposed model. At this point, there is no spatial energy variation within a room. The difference of energy level between the rooms is due to the size of the coupling area and the overall absorption of each room.
- (2) Addition of sound energy density depending on source-receiver distance in the main room, according to parameter  $a$ . This term introduces the first effect relative to sound energy variation, according to source-receiver distance.
- (3) Addition of sound energy density relative to the energy returned from the adjoining volumes, depending on aperture-receiver distance and corresponding to an additional slope within the energy decay curve. This term also influences spatial energy variation in the main room.
- (4) Normalization of the obtained energy decay curve.

The numerical implementation used in the present study relies on Eq. (16), accounting for each of the aforementioned points in the case of two coupled rooms

$$w(\mathbf{r}, t) = E_{01} \left( \frac{a}{r_{\text{SR}}} \exp(-\varepsilon r_{\text{SR}}) + b \right) \exp(-\sigma_1 t) + E_{02} \left( \frac{a}{r_{\text{AR}}} \exp(-\varepsilon r_{\text{AR}}) + b \right) \exp(-\sigma_2 t), \quad (16)$$

where  $E_{0i}$  are the initial sound energy levels in each room estimated by Cremer's approach<sup>5</sup> in steady state,  $r_{\text{SR}}$  and  $r_{\text{AR}}$  are the source-receiver and aperture-receiver distances, respectively,  $\sigma$  is the temporal energy decay rate, and  $\varepsilon = \sqrt{(\sigma/D)}$  stands for the spatial decay rate with  $\sigma$  and  $D$  defined in Eqs. (2) and (3). Coefficients  $a$  and  $b$  were estimated by comparing spatial energy variation over the 30 receiver positions with scale model measurements in a single room configuration so that the model matches the measured energy. In the present case, the relative value of these coefficients is  $a = 50b$ . In fact, these parameters are used to express the relative importance of spatial and temporal decaying exponential terms. Thus, configuring the model can be done by fixing  $b$  and varying  $a$  so that the model best matches measurements.

An example is performed for a rectangular main room whose architectural and acoustical specifications are listed in Table I and illustrated in Fig. 1. The coupling area is  $S_c = 137 \text{ m}^2$  which is 3% of the total surface of the main room ( $S_1 = 4560 \text{ m}^2$ ) and 32% of the area of the wall ( $S_w = 432 \text{ m}^2$ ) separating the main room and the chamber. This configuration results in a clearly curved temporal energy decay and a noticeable sound level variation

TABLE I. Architectural specifications of the main room and reverberation chamber for the numerical simulation (full scale [1:1]) and the scale model (scale 1:20): length (L), width (W), height (H), volume (V), surface area (S), mean absorption coefficient ( $\bar{\alpha}$ ), and RT in the 500 Hz octave band.

| Scale                 | L (m) | W (m) | H (m) | V (m <sup>3</sup> ) | S (m <sup>2</sup> ) | $\bar{\alpha}$ | RT (s) |
|-----------------------|-------|-------|-------|---------------------|---------------------|----------------|--------|
| Main room             |       |       |       |                     |                     |                |        |
| 1:1                   | 44    | 24    | 18    | 19 000              | 4560                | 0.38           | 1.53   |
| 1:20                  | 2.2   | 1.2   | 0.9   | 2.38                | 11.4                | 0.38           | 0.08   |
| Reverberation chamber |       |       |       |                     |                     |                |        |
| 1:1                   | 14    | 24    | 18    | 6050                | 2040                | 0.10           | 8.39   |
| 1:20                  | 0.7   | 1.2   | 0.9   | 0.76                | 5.1                 | 0.10           | 0.42   |

throughout the considered space. Figure 1 shows the results of this example, where the reverberation chamber is placed on one side of the main room as often encountered in coupled volume concert halls. A map of sound energy level as well as the temporal sound energy decay at a chosen point and spatial sound energy decay along a line of receivers can be determined. The same calculation can be repeated for various aperture sizes or for additional secondary volumes in order to obtain sound energy decays with more than two slopes.

### III. QUANTIFICATION OF NON-EXPONENTIAL IMPULSE RESPONSES

Precise quantification of non-exponential impulse responses is necessary for their characterization and in order to compare various cases. This study employs the Marching Line method<sup>29</sup> to estimate appropriate acoustical parameters. These quantifiers are the decay time ( $DT_i$ ) of each slope within the curved decay, evaluated to  $-60 \text{ dB}$ , and the time and level ( $BP_t$ ,  $BP_L$ ) of the point on the decay curve between consecutive slopes, called the bending point, as illustrated in Fig. 2. The method is based on a recursive algorithm which calculates root-mean-square (rms) deviations between Schroeder's backward integration<sup>30</sup> [or reverse integrated curve (RIC), Eq. (17)] of impulse responses expressed in decibels and step-wise linear regressions. The RIC is calculated as follows:

$$\text{RIC}(\mathbf{r}, t) = \int_t^\infty p^2(\mathbf{r}, \tau) d\tau, \quad (17)$$

where  $p$  is the sound pressure of an impulse response. The first point of the RIC is defined as the point at  $-0.1 \text{ dB}$  below the maximum of the normalized RIC. Linear regressions are successively estimated between this point and a progressively descending point at each iteration, increasing the length of the linear regression. The rms deviation between the RIC and the linear regression also increases until a threshold is reached and iterations are stopped. The linear regression is then stored as a detected straight portion of the RIC if it decays over a minimum of  $10 \text{ dB}$  to ensure a substantial slope. If it is not the case, input parameters of the algorithm have to be changed. The starting point for the second slope is defined at  $10 \text{ dB}$  below the last point of the first slope in order to avoid the curved part of energy decay

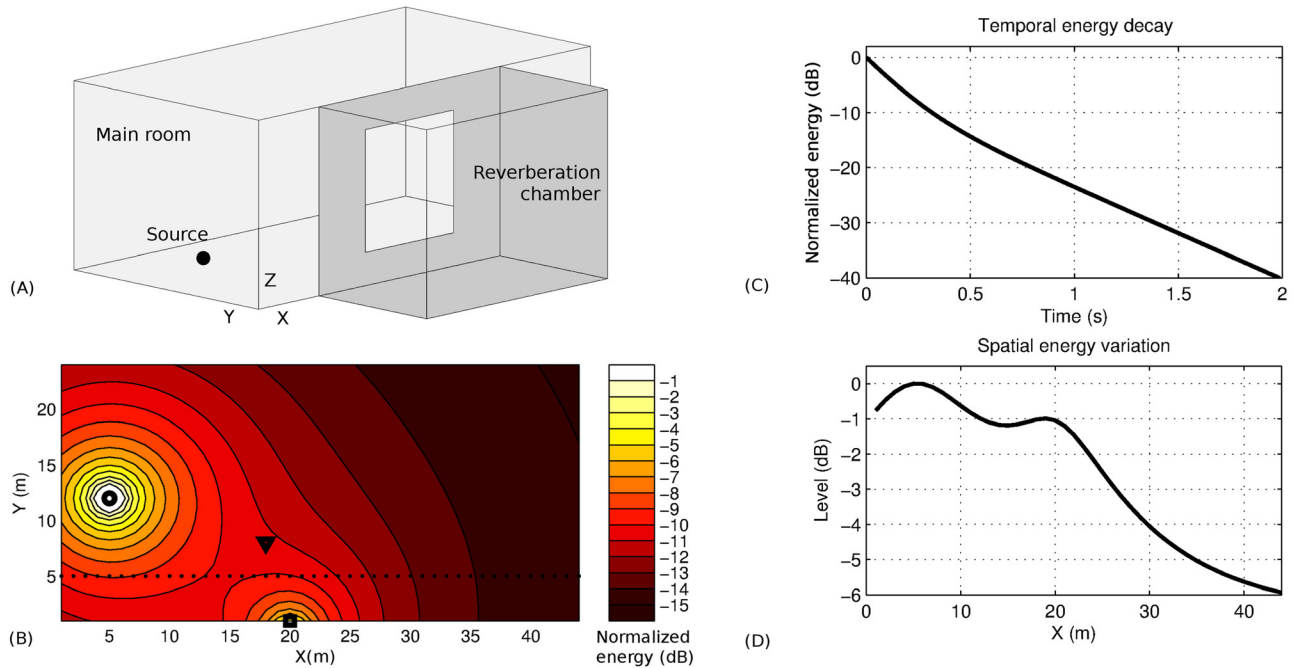


FIG. 1. (Color online) (A) Perspective of the coupled volume hall's geometry. Corresponding specifications are in Table I. (B) Map of normalized sound energy level on a horizontal plan in the rectangular main room. The surface coupling the main room to a reverberation chamber is the square ( $X=20$ ;  $Y=0$ ). Sound source is represented by a circle ( $X=5$ ;  $Y=12$ ). (C) Temporal energy decay at the triangle position ( $X=18$ ;  $Y=8$ ). (D) Spatial energy variation along the dotted line ( $Y=5$ ).

curve. Iterations are then calculated in the same manner until the rms deviation threshold is reached again. Bending points are estimated as the closest point on the decay curve to the intersection point of these successive linear regressions.

#### IV. COMPARISON OF THE MODEL TO MEASUREMENTS AND SIMULATIONS

Predictions from the proposed model have been compared to measurements in an acoustical scale model and simulations achieved with CATT-Acoustic software (version v9.0a, TUCT v1.0g release). Various configurations of source-receiver arrangement and coupling area have been investigated. Special attention was paid to temporal energy decays at various receiving points, including near and far positions relative to the sound source as well as total energy variation through the space. Comparisons are quantified

using rms deviation for various quantities according to the following equation:

$$D_{\text{rms}} = \sqrt{\frac{1}{N} \sum_{i=1}^N (X(\mathbf{r}_i) - X_{\text{ref}}(\mathbf{r}_i))^2}, \quad (18)$$

with  $N$  the number of receivers,  $X$  the compared value, and  $X_{\text{ref}}$  the reference, or standard value. In the following,  $X$  is either one of the acoustical parameters or the total energy value.

#### A. Physical and digital models

The architectural model has dimensions and acoustical characteristics (Table I) of a typical large concert hall, although the reverberation time (RT) is quite high in the chamber, as compared to generally encountered values in coupled volume concert halls.<sup>31</sup> The differences with the earlier example in Sec. II D is the location of the reverberation chamber, here placed behind the stage, and the fact that opposing walls are not perfectly parallel. This position for the reverberation chamber was chosen to highlight the effects of source/receiver/aperture distance variations, as the source could be placed at either end of the model without altering the alignment configurations of all other elements. The hall has a shoebox-like overall geometry, at full scale and 1:20 scale for the numerical and physical models, respectively. The plans in Fig. 3 show that most opposite walls are not parallel but are slightly angled ( $5^\circ$ ) in order to avoid flutter echoes. While the floor and ceiling in the main room are parallel, large curved rigid reflectors have been installed close to the ceiling in the scale model, as shown in

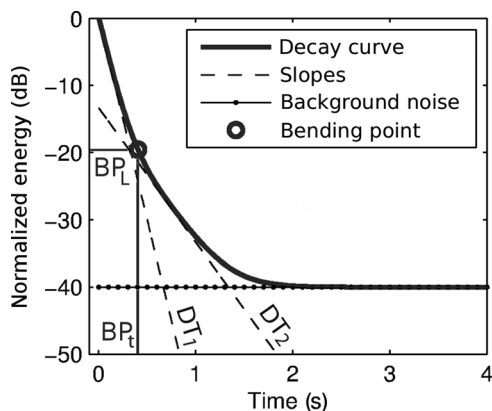


FIG. 2. Acoustical parameters describing a multi-slope energy decay curve presented in the case of two slopes.

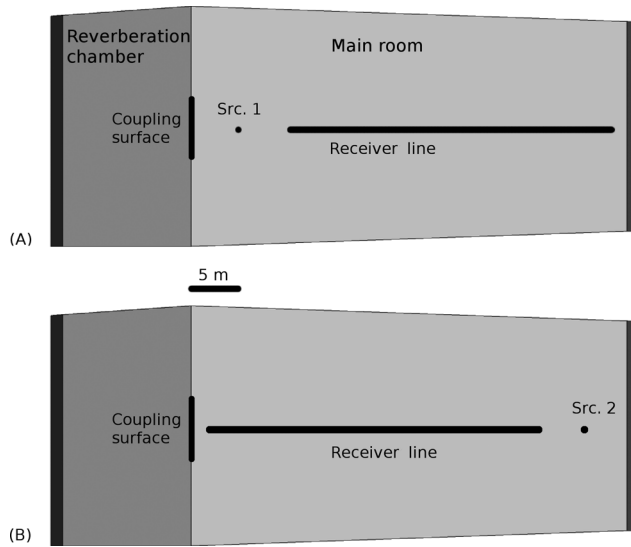


FIG. 3. Floor plan of the geometry used for ray-tracing simulation and measurements in the 1:20 scale model. Src. 1 and Src. 2 are presented in plans (A) and (B), respectively. Coupling area is represented by a thick line on the separating wall. The large dark lines at the end of each room represent the tilted walls which are not exactly vertical in order to avoid flutter echoes. Opposite boundaries present an angle of  $5^\circ$ .

Fig. 4, to increase sound diffusion within the room. No additional features such as balconies were included so that the model represented general coupled spaces.

For the scale model, the sound source was a miniature dodecahedral loudspeaker array (model 3D-032, Dr-Three), the receivers were DPA 4060 microphones, and the audio interface was a RME Fireface 800. While this data acquisition system was designed to work within the audible frequency range, it provided a usable signal up to 50 kHz, corresponding to the frequency band centered on 2 kHz at full scale. This equipment has been used in previous acoustical studies, including measurements in the scale model of the future Philharmonie de Paris concert hall.<sup>32</sup> The obtained signal-to-noise ratio was greater than typically achievable by classical scale model measurement equipment, which is extremely important when studying coupled space acoustics and to detect late slopes at low energy levels. Due to both the upper frequency limit caused by scale model measurements, the lower frequency limit caused by the use of ray-tracing, and the fact that coupling effect is stronger at low- and mid-frequencies, this study therefore only compares results for the 500 Hz centered octave band.

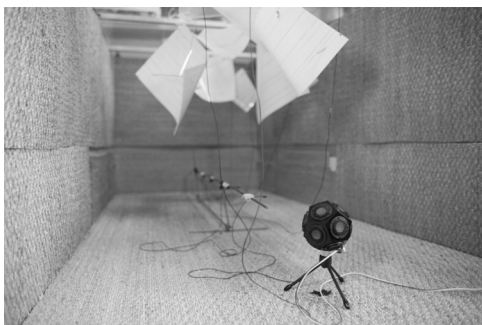


FIG. 4. Photograph of the main room of the scale model with the miniature dodecahedron source at Src. 1 and the microphone alignment.

TABLE II. Specifications of materials, mean absorption coefficient, and RTs in uncoupled rooms in ray-tracing simulations in the 500 Hz octave band. Mat 1 is Plexiglas/PVC, Mat 2 are Braided fibers, and Mat 3 is Wood (MDF).

|                           | Main room |       | Reverb. Chamber |       |
|---------------------------|-----------|-------|-----------------|-------|
|                           | Mat 1     | Mat 2 | Mat 1           | Mat 3 |
| $\alpha$                  | 0.03      | 0.50  | 0.03            | 0.06  |
| Surface (m <sup>2</sup> ) | 1440      | 3070  | 1000            | 1020  |
| $\bar{\alpha}$            | 0.35      |       | 0.05            |       |
| RT (s)                    | 1.55      |       | 8.26            |       |

The numerical model reproduced the scale model specifications in terms of dimensions and wall absorption, as presented in Table II. The wall absorption was defined per octave band so that RTs matched those calculated from measurements in the uncoupled rooms. The assumption was made that the scale model was globally highly diffusive because walls were covered by a material made of braided fibers presenting depth variations of 0.8 cm, which is a quarter wavelength at 10 kHz (i.e., 500 Hz at 1:20 scale). In addition, the large curved reflectors increased the diffusion of sound field in the scale model. Therefore, in ray-tracing simulations where these reflectors did not appear, wall surfaces were assigned Lambert coefficients as high as feasible, up to 70% as the maximum value as recommended by Rindel.<sup>33</sup> Scattering was also taken into account for the first order reflections (“max split-order=1”). As a result, both scale model, ray-tracing simulations, and the diffusion model presented a high level of sound diffusion so that comparisons were possible between one another.

CATT-Acoustic v9.0a, TUCT v1.0g release, proposes three different algorithms, increasing the results precision, to handle acoustic simulations in various venues. The number of rays is an important issue when dealing with coupled spaces because a sufficient number must enter the secondary chamber to provide a second slope in the energy decay. A preliminary comparison between impulse responses conducted from measurements and simulations using  $10^5$  and  $10^6$  rays per octave bands in TUCT’s algorithm 1, and  $10^5$  rays in algorithm 2, all other conditions remaining unchanged, has shown that results were closer to measurements when using  $10^6$  rays with algorithm 1. These settings were chosen for the present study. Results presented here focus on the octave band centered on 500 Hz which is a compromise between mid- and low-frequencies where coupling effect is stronger, providing clear observations of the encountered phenomena.

## B. Source-receiver arrangements

The sound source was placed at one end of the main room, which represents the stage location. Two configurations have been tested: The source placed next to the coupling area (referred to as configuration Src. 1), 5 m away from it, and at the opposite end (Src. 2), 5 m away from the rear wall, as illustrated in Fig. 3. These configurations allowed for testing various relative proportions of time delay

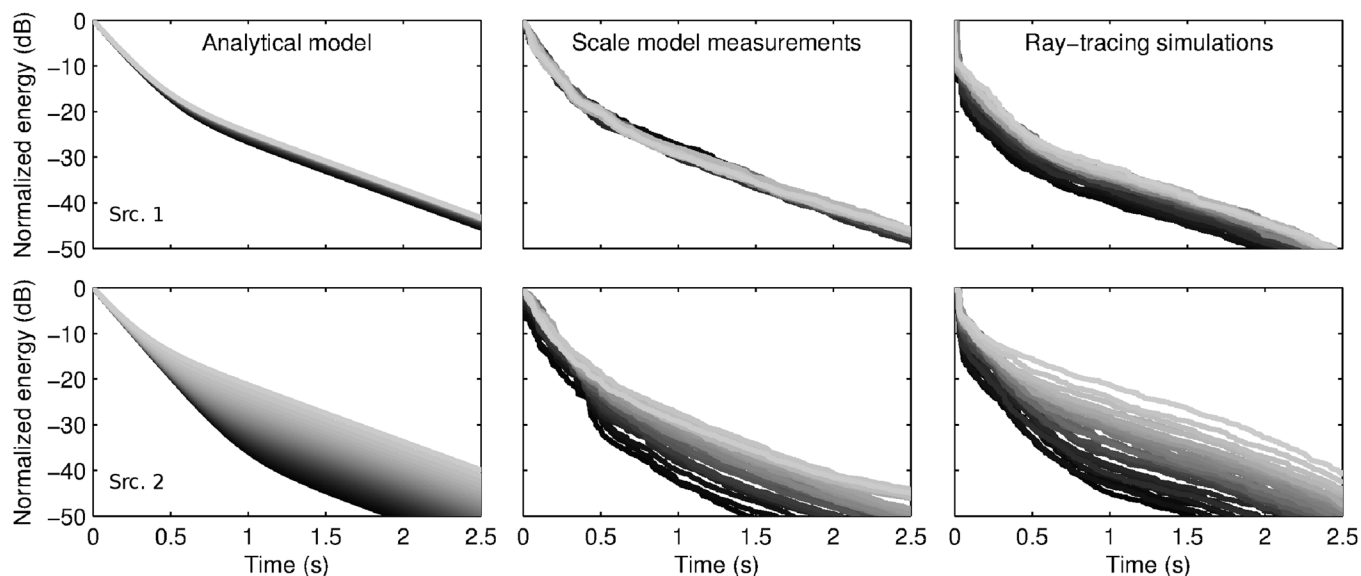


FIG. 5. Time-energy decay curves in the 500 Hz octave band from the analytical model, measurements in the scale model, and ray-tracing simulations. Darker curves represent receivers near the sound source and the lighter the curve, the greater the source-receiver distance. Top row: Source near the coupling area as illustrated in Fig. 3 (Src. 1). Bottom row: Source on the side opposite to the coupling area (Src. 2).

and sound energy level between the direct sound and late reverberation from the chamber, depending on the receiver location. A total of 30 receivers were placed with 1 m step along the line represented in Fig. 3, allowing for measurements with source-receiver distances from 7 to 36 m in order to observe the effect of distance between the triplet of source, coupling area, and receiver since the proposed analytical model includes distance variation. The square coupling area was set to  $S_c/S_1 = 1\%$  in order to provide energy decay curves with two distinct slopes.

### 1. Sound energy decays

Figure 5 shows the temporal energy decay curves estimated by the proposed analytical model as well as those from measurements and numerical simulations for the two sound source positions, individually normalized. In both cases, the second slope increases in level with increasing source-receiver distance (from darker to lighter curves). Furthermore, the main difference observed by the change of source position is the variation in late energy decay levels. If the source is placed near the coupling area (upper row in Fig. 5), the second slope of the energy decay curves obtained along the line of receivers lie within a range of 10 dB of dynamics. This range of levels is much greater if the source is placed at the opposite side of the room (lower row in Fig. 5). This difference of dynamics can be explained by the time required for sound energy to reach the chamber from source position 1 or 2 and then to reach receivers from the chamber.

### 2. Acoustical parameters

The resulting energy decay curves have been analyzed using the previously mentioned Marching Line method which estimates acoustical parameters adapted to multi-slope decays. Figure 6 shows the results for early and late decay times ( $DT_1$  and  $DT_2$ ) as well as the bending point time and level ( $BP_T$  and  $BP_L$ ) for each receiver.

Decay times are difficult to analyze precisely on the jagged energy decays obtained from measurements and simulations. Results present a degree of variability between successive receivers while no particular tendency is found. Table III shows the standard deviation for the series of acoustical parameters and the numerical simulations appear to be more variable than measurements, particularly for  $DT_1$  and  $DT_2$ . Standard deviation for the analytical model is smaller, as compared to measurements and ray-tracing simulations. The analytical model presents almost constant decay times over all receivers because its temporal decay rates, governed by the argument of the temporal decaying exponential in Eq. (4), are based on the classical statistical theory for which the temporal decay rate is homogeneous throughout the volume and depends on architectural parameters only.

Bending point results show different trends depending on source position. While the bending point does not vary much in the time-level space when the sound source is near the coupling area (Src. 1), strong variations are observed when the source is placed at the opposite end of the room (Src. 2). The trend observed in Fig. 5 is confirmed by acoustical parameters in Fig. 6 and certain agreement is found between the proposed model, measurements, and ray-tracing simulations, especially for estimation of the bending point level, as shown in Table IV, where rms deviations for the acoustical parameters are presented.  $BP_T$  of the analytical model is generally greater than values of measurements and simulations, except at the furthest receivers in the scale model, and follow the same decreasing tendency at Src. 2. This means that the second slope appears later in time for the analytical model. The arrival time of the second slope is determined by its initial level and the decay rate is estimated by Sabine's theory. Hence the observed time difference might be due to the initial level estimation in each room which is based on distances between the source, receiver, and coupling area. If the receiver is close to the source and

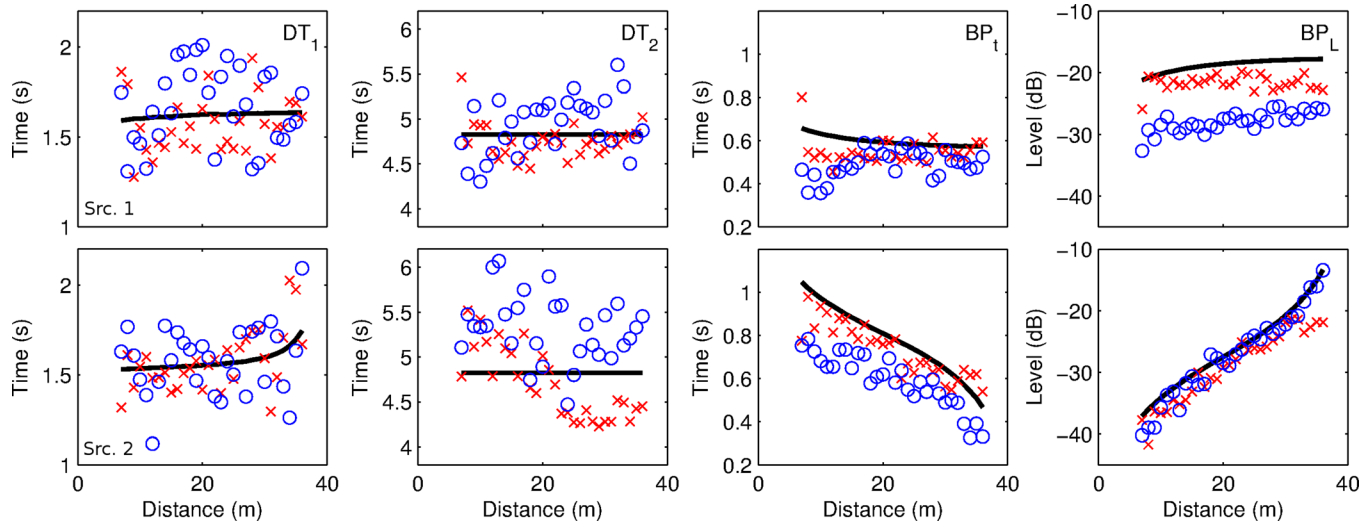


FIG. 6. (Color online) Acoustical parameters in the 500Hz octave band at each receiver position from the analytical model (solid line), measurements in the scale model ( $\times$ ), and ray-tracing simulations ( $\circ$ ).  $DT_1$  and  $DT_2$  are the decay times of the early and late slopes of curved sound decays,  $BP_t$  and  $BP_L$  are the bending point time and level, respectively. Top row: Source near the coupling area (Src. 1). Bottom row: Source on the opposite side to the coupling area (Src. 2).

far from the aperture, the second slope will appear later than in the case of a receiver closer to the aperture. The aperture is approximated here as a point source, placed at the center of the modeled coupling area. The observed discrepancies for  $BP_t$  might also be due to a slight overestimation of spatial decrease of sound energy.

Results for  $BP_L$  are in good agreement, especially for the analytical model and ray-tracing simulations in configuration Src. 2. In configuration Src. 1, the bending point is found at a lower level for simulations than for measurements and the analytical model because of the stronger direct sound, observable in Fig. 5, which lowers the decay curves by about 10 dB. This level also corresponds to the difference observed in  $BP_L$  values.

The rms deviation values in Table IV show that the closest couple within the triplet analytical model/measurements/numerical simulations is “Mod./Meas.” for Src. 1 and “Sim./Mod.” or “Mod./Meas.” for Src. 2 depending on the parameter. This confirms the visual information in Fig. 6: Results from the analytical model lie between those from measurements and numerical simulations, which tends to validate the use of this model in coupled volume geometry.

A previous study<sup>23</sup> has compared coupled room scale model measurements and numerical resolution of the diffusion equation. The obtained bending point times ( $BP_t$ )

exhibited differences on the order of a few mean free times (MFTs, time required to travel the mean free path  $\lambda = 4V/S$ ). The results of the present study are in agreement: The average difference of  $BP_t$  from the model and from measurements and simulations is 112 ms, which is about 2 MFT ( $\lambda = 17$  m, MFT = 49 ms). As mentioned in the previous study, this time interval is of the same order as the early reflections duration, before reverberation occurs. The main difference with the present study lies in the fact that  $BP_t$  is longer for measurements, whereas here  $BP_t$  is longer for the diffusion model.

### 3. Total energy

Total sound energy can be calculated at each receiver position as the sum of squared sound pressure of the whole impulse response. In order to compare impulse responses from measurements and ray-tracing simulations with the analytical model which does not provide impulse responses but energy decay curves, the total sound energy is estimated as follows, based on the RIC:

$$E(\mathbf{r}) = 10 \log_{10} \text{RIC}(\mathbf{r}, t), \quad (19)$$

TABLE III. Standard deviation of acoustical parameters calculated from linear regressions over all 30 receivers for Src. 1 and Src. 2 (Fig. 6) from measurements and ray-tracing simulations.

|   | $DT_1$ (s) | $DT_2$ (s) | $BP_t$ (s) | $BP_L$ (dB) |
|---|------------|------------|------------|-------------|
| Src. 1 - Source near coupling area        |            |            |            |             |
| Measurements                              | 0.16       | 0.19       | 0.06       | 1.18        |
| Simulations                               | 0.22       | 0.29       | 0.06       | 1.02        |
| Src. 2 - Source opposite to coupling area |            |            |            |             |
| Measurements                              | 0.14       | 0.22       | 0.05       | 1.37        |
| Simulations                               | 0.19       | 0.35       | 0.05       | 1.40        |

TABLE IV. RMS deviation of acoustical parameters (Fig. 6) and total energy (Fig. 7) between couples of the triplet analytical model (Mod.)/measurements (Meas.)/ray-tracing simulations (Sim.) over all receivers.

|   | $DT_1$ (s) | $DT_2$ (s) | $BP_t$ (s) | $BP_L$ (dB) | E (dB) |
|---|------------|------------|------------|-------------|--------|
| Src. 1 - Source near coupling area        |            |            |            |             |        |
| Mod./Meas.                                | 0.17       | 0.20       | 0.08       | 3.19        | 0.8    |
| Sim./Meas.                                | 0.31       | 0.42       | 0.11       | 6.55        | 0.9    |
| Sim./Mod.                                 | 0.22       | 0.32       | 0.13       | 9.23        | 0.5    |
| Src. 2 - Source opposite to coupling area |            |            |            |             |        |
| Mod./Meas.                                | 0.14       | 0.41       | 0.09       | 3.40        | 1.3    |
| Sim./Meas.                                | 0.26       | 0.74       | 0.16       | 3.02        | 1.7    |
| Sim./Mod.                                 | 0.18       | 0.61       | 0.20       | 1.73        | 0.7    |

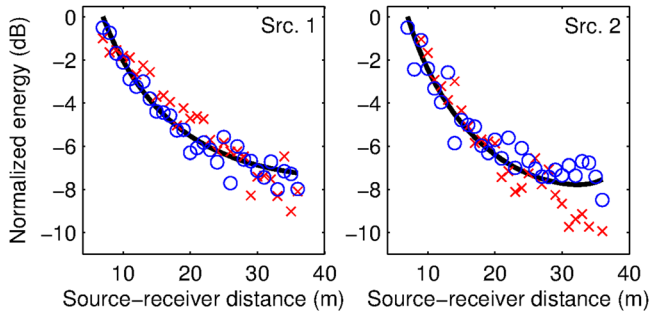


FIG. 7. (Color online) Total energy at each receiver position for the analytical model (solid line), measurements in the scale model ( $\times$ ), and ray-tracing simulations ( $j$ ). Src. 1 stands for the source position near the coupling area and Src. 2 for the source being on the opposite side to coupling area.

where RIC can be either energy density from the model or backward integration of squared sound pressure of impulse responses from measurements and ray-tracing simulations. The rms deviations presented in Table IV for comparison of two elements of the triplet [analytical model/measurements/ray-tracing simulations] are on the order of 1 dB. The smallest differences are found in configuration Src. 1 where rms deviation values are inferior to 1 dB. For both Src. 1 and Src. 2, the analytical model is closer to numerical simulations in terms of rms deviation. The spatial energy decay is presented in Fig. 7 for both sound source positions. Results cannot be compared to Barron’s Revised Theory<sup>9</sup> because the latter is only valid for single uncoupled enclosures as it does not account for the amount of energy returned from the chamber back to the main room. The energy evolution as a function of distance is similar between the analytical model and numerical simulations exhibiting curved profiles while measurement results present a linear evolution in configuration Src. 1. The behavior of sound energy is also different for receivers distant from the source in configuration Src. 2, which are nearer to the chamber aperture. Energy returned back from the chamber in this area, where energy fluxes cross<sup>34</sup> and diffraction phenomenon are likely to happen near the coupling area edges, is modeled by different methods, based on statistical or geometrical acoustics, and therefore leads to different results.

### C. Coupling area variation

Several sizes of aperture have been tested in order to compare the analytical model with measured and simulated data. The coupling aperture area can be expressed as a percent of the inner surface of the main room as well as a percent of the separating wall between the main room and the reverberation chamber. Two sizes of aperture were tested in the scale model, with  $S_c = 0.5\%$  and  $1\%$  of the main room surface area  $S_1$ . Larger coupling areas have been implemented with the proposed model as well as with ray-tracing to extend the tested range up to  $S_c/S_1 = 4\%$ . The source was 5 m from the coupling area and 5 m to the side of the central axis of the room, at coordinates ( $X = 5; Y = 17$ ). A total of six receivers were placed along the center line (see Fig. 3) at 6 m intervals, the first receiver at 7 m from the sound source. Source-receiver distances therefore varied from 7 to 37 m.

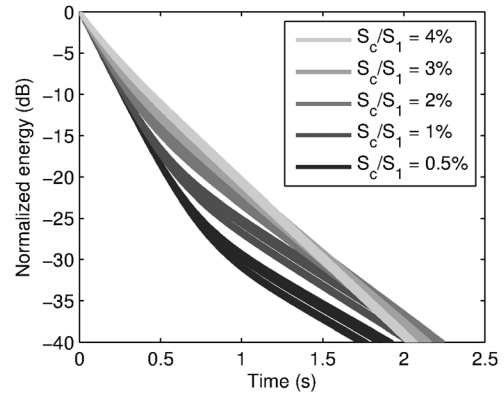


FIG. 8. Temporal energy decays for various coupling area conditions from 0.5% to 4% of the main room surface at six receiver positions between 7 and 37 m from the source. Data from the analytical model.

Results from the analytical model (see Fig. 8) show that smaller coupling areas (darker curves) lead to temporal energy decay curves with two distinct slopes of different decay rates, the second slope appearing at lower level, between  $-20$  and  $-30$  dB in this example. In contrast, larger coupling areas (lighter curves) induce decay curves with slopes similar to each other, having bending points at higher levels. Increasing the coupling area asymptotically would lead to a large single volume, providing a straight energy decay curve. However, a slight double slope could be obtained as it has been observed in single volume halls because of the inhomogeneity of absorbing material distribution throughout space.<sup>35</sup> Decreasing the coupling area asymptotically would create a smaller single volume room.

Quantification of the calculated and measured decay curves is presented in Fig. 9 and in Table V, showing the range of variation of acoustical parameters as a function of coupling area, with measurement results available for only two of the coupling areas. The early and late decay times ( $DT_1$  and  $DT_2$ ), averaged over the six receiver positions in Table V, show various tendencies. With increasing coupling area,  $DT_1$  increases and  $DT_2$  decreases. A variation span of 0.8 and 2.1 s for the analytical model, and 0.7 and 2.8 s for ray-tracing simulations due to coupling area was observed. Considering the smallest values, relative variations of 50% and 39% are obtained for  $DT_1$ ; 64% and 86% for  $DT_2$ , for the analytical model and ray-tracing simulations, respectively. These relative variations are much higher than the perceptual threshold for RTs above 1 s, as reported by Seraphim<sup>36</sup> for single slope reverberation, which is 5% of the RT value. Hence, the change in sound field induced by such modifications of the coupling area is certainly audible and can be used to alter the audible environment.

Bending point time and level are also modified by the coupling area changes. Increasing the coupling area causes the bending point time to arrive earlier and consequently the bending point level to be higher (Fig. 9). This variation pattern has been observed with the source-receiver distance variations in Fig. 6 while decay times did not vary much since global absorption was unchanged in the two volumes. In actuality, changing the coupling area modifies the wall surface in each volume and thus alters the inner total absorption.

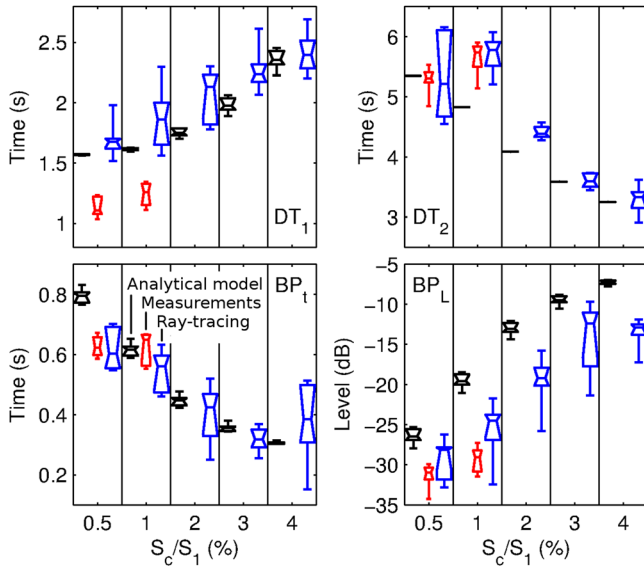


FIG. 9. (Color online) Boxplots of acoustical parameters in various coupling area cases from 0.5% to 4% of the main room surface, i.e., each column, from the analytical model (left), scale model measurements (center), and ray-tracing simulations (right), calculated from the energy decay curves in Fig. 8. Measurements were performed only for  $S_c/S_1 = 0.5\%$  and  $1\%$ .

Therefore, decay times for each receiver vary more as a result of changes in coupling area than due to modifying the source-receiver distance.  $BP_t$  shows particularly good agreement, both in terms of low rms deviations and evolution tendency. The latter is also true for  $BP_L$ , although measurement results showed globally lower levels. In addition, parameter values at  $S_c/S_1 = 1\%$  can be compared to those in Sec. IV B presenting the analytical model, where the same coupling area was used. The observed parameter values are not exactly identical, although discrepancies are small (similar to standard deviation values in the series of 30 receivers,

TABLE V. Acoustical parameters averaged over the six receiver positions, for various coupling areas.  $S_1 = 4560 \text{ m}^2$  is the total surface area of the main room,  $S_w = 432 \text{ m}^2$  is the area of the separating wall between the main room and the reverberation chamber.

| $S_c$ ( $\text{m}^2$ )  | 22.8  | 45.6  | 91.2  | 136.8 | 182.4 |
|-------------------------|-------|-------|-------|-------|-------|
| $S_c/S_1$ (%)           | 0.5   | 1     | 2     | 3     | 4     |
| $S_c/S_w$ (%)           | 5     | 11    | 21    | 32    | 42    |
| Analytical model        |       |       |       |       |       |
| $DT_1$ (s)              | 1.6   | 1.6   | 1.8   | 2.0   | 2.4   |
| $DT_2$ (s)              | 5.4   | 4.8   | 4.1   | 3.6   | 3.3   |
| $BP_t$ (s)              | 0.79  | 0.62  | 0.45  | 0.36  | 0.31  |
| $BP_L$ (dB)             | -26.4 | -19.5 | -13.1 | -9.5  | -7.3  |
| Measurements            |       |       |       |       |       |
| $DT_1$ (s)              | 1.1   | 1.2   |       |       |       |
| $DT_2$ (s)              | 5.3   | 5.6   |       |       |       |
| $BP_t$ (s)              | 0.63  | 0.63  |       |       |       |
| $BP_L$ (dB)             | -31.4 | -29.3 |       |       |       |
| Ray-tracing simulations |       |       |       |       |       |
| $DT_1$ (s)              | 2.1   | 1.8   | 1.9   | 2.0   | 2.5   |
| $DT_2$ (s)              | 6.0   | 5.9   | 4.5   | 3.7   | 3.2   |
| $BP_t$ (s)              | 0.70  | 0.54  | 0.39  | 0.29  | 0.28  |
| $BP_L$ (dB)             | -24.1 | -18.8 | -13.2 | -9.8  | -8.5  |

presented in Table III). Differences are likely due to differences in source position, which modifies the distance between source and coupling area, changing the amount of energy which enters the reverberation chamber, and more generally alters the temporal and spatial distribution of sound reflections within the space.

## V. DISCUSSION

Comparing the proposed analytical model with other methods for estimating coupled sound fields characteristics, e.g., ray-tracing used in this study or finite element method used in previous research,<sup>17</sup> leads to several advantages and drawbacks. The room's geometry is taken into account through the diffusion coefficient which depends on the mean free path. This coarse descriptor of the space is less precise than a ray-tracing model but contributes to the fact that the proposed method requires much shorter calculation times. Frequency dependence is found in the definition of absorption coefficients, in the same manner as for ray-tracing methods, but different than wave-based methods where complex wall impedances are defined. Calculation of impulse responses at every position in the space is not required since a solution equation is used as opposed to a partial differential equation and issues relating to mesh geometry encountered in wave-based methods are avoided. Certain physical details can be missed since the method is based on statistical acoustics, which considers global absorption, and diffraction does not appear in the proximity of edges. Although distance between source, receiver, and coupling area is taken into account, distance from a receiver to the walls does not influence the results, which can be an issue in certain cases. However, comparisons performed here show that the proposed model provides a level of reliability comparable to the ray-tracing method, particularly for  $S_c/S_1 > 2\%$  as shown in Fig. 9 and mentioned in Sec. IV C, and it would be interesting to conduct further comparisons with wave-based methods. The range of available coupling areas in real halls being up to 10% of the main room surface area or more, the typically used coupling area is larger than 2% in order to let a sufficient amount of sound energy enter the chamber. Hence, the range of coupling area where comparisons are in agreement in this study meets the used range in real coupled volume concert halls.

In the proposed model, the coupling area is represented as a single point, alternatively acting as receiver and secondary source. This representation can be an issue when the coupling area is large compared to the distance to the primary source or receivers. An alternative modeling would consist in discretizing the surface by a number of distributed points which receive and return sound energy from one volume to the other. This coupling area modeling would be closer to reality in coupled volume concert halls, where coupling areas are composed of several doors, opened next to each other in an enormous multitude of possible combinations.

## VI. CONCLUSION AND PERSPECTIVES

The proposed model of sound energy behavior adapted to coupled spaces allows for estimating both temporal and spatial components of sound fields. Accounting for

architectural data, this model based on the diffusion equation enables estimation of sound energy levels under steady state excitation at any point within the considered space as well as temporal sound energy decays corresponding to stopped source excitation. This model has been compared to scale model measurements and ray-tracing simulations for validation. Comparisons were performed on acoustical parameters which describe multi-slope energy decays as well as total energy level. Several acoustical issues are tested with the three different methods: The influence of distance between sound source, receiver, and coupling area as well as coupling area variations. Through rms deviation analysis, the analytical model was generally found to lie between measurements and ray-tracing simulations in the generally used range of coupling area, showing a sufficient level of reliability and accuracy to handle the general prediction of sound field behavior in coupled spaces.

Possible applications of the proposed analytical model are mainly prediction tools for acoustical designers who build spaces as well as operators of such spaces, e.g., concert hall managers. These can consist in quantifying sound fields in coupled volume concert halls or sound levels in large factories with noisy engines in several connected rooms. However, since statistical acoustics is used, the proposed analytical model can be applied to large volumes only, where the Schroeder frequency<sup>37</sup> is low, and does not allow for considering modal behavior in smaller volumes, as often encountered in recording studios. One can also imagine using this model to rapidly synthesize room impulse responses by applying the temporal decays generated by the present procedure to noise, with varying position and coupling details, as has been previously proposed.<sup>38</sup> This allows performing auralization in virtual coupled spaces, which could be used in architectural design and virtual reality applications for providing realistic real-time sound field behavior at a low computational cost.

Further research includes testing various conditions of sound absorption in each room in order to study the influence of initial individual RT on the coupled impulse response. An implementation of more general cases could be performed, with several coupling areas between the main room and different reverberation chambers. Furthermore, comparisons could be performed between this analytical approach and methods of numerical resolution, in particular regarding the spatial distribution of absorption throughout a room.

## ACKNOWLEDGMENTS

The authors would like to thank Renaud Leblanc-Guindon for the scale model measurements, and Philippe Néméh for the photograph of the scale model.

<sup>1</sup>W. C. Sabine, *Collected Papers on Acoustics* (Harvard University Press, Cambridge, 1922), 279 p.

<sup>2</sup>A. H. Davis, "Reverberation equations for two adjacent rooms connected by an incompletely sound-proof partition," *Philos. Mag.* **50**, 75–80 (1925).

<sup>3</sup>C. F. Eyring, "Reverberation time measurements in coupled rooms," *J. Acoust. Soc. Am.* **3**, 181–206 (1931).

<sup>4</sup>H. Kuttruff, *Room Acoustics* (Elsevier Science Ltd., London, 1973), 452 p.

<sup>5</sup>L. Cremer, H. A. Müller, and T. J. Schultz, *Principle and Applications of Room Acoustics* (Applied Science, New York, 1982), 651 p.

<sup>6</sup>C. D. Lyle, "The prediction of the steady state sound levels in naturally coupled enclosures," *Acoust. Lett.* **5**, 16–21 (1981).

<sup>7</sup>J. Jouhaneau, *Acoustique des Salles et Sonorisation (Room Acoustics and Sound Systems)* (Collection CNAM, Lavoisier, Paris, 1997), 610 p.

<sup>8</sup>J. E. Summers, R. R. Torres, and Y. Shimizu, "Statistical-acoustics models of energy decay in systems of coupled rooms and their relation to geometrical acoustics," *J. Acoust. Soc. Am.* **116**, 958–969 (2004).

<sup>9</sup>M. Barron and L. J. Lee, "Energy relations in concert auditoriums," *J. Acoust. Soc. Am.* **84**, 618 (1988).

<sup>10</sup>J. E. Summers, "Accounting for delay of energy transfer between coupled rooms in statistical-acoustics models of reverberant-energy decay," *J. Acoust. Soc. Am.* **132**(2), EL129–EL134 (2012).

<sup>11</sup>F. Martellotta, "A multi-rate decay model to predict energy-based acoustic parameters in churches (L)," *J. Acoust. Soc. Am.* **125**, 1281–1284 (2009).

<sup>12</sup>P. Luizard, N. Xiang, J. D. Polack, and B. F. G. Katz, "Coupled volumes and statistical acoustics: Preliminary results of an improved analytical model (A)," *J. Acoust. Soc. Am.* **131**, 3245 (2012).

<sup>13</sup>F. Ollendorff, "Statistical room-acoustics as a problem of diffusion: A proposal," *Acta Acust. Acust.* **21**, 236–245 (1969).

<sup>14</sup>J. Picaut, L. Simon, and J. D. Polack, "A mathematical model of diffuse sound field based on a diffusion equation," *Acta. Acust. Acust.* **83**, 614–621 (1997).

<sup>15</sup>P. Morse and H. Feshbach, *Methods of Theoretical Physics* (McGraw Hill, New York, 1978), 1953 p.

<sup>16</sup>J. M. Navarro, F. Jacobsen, J. Escolano, and J. J. Lopez, "A theoretical approach to room acoustic simulations based on radiative transfer model," *Acta Acust. Acust.* **96**, 1078–1089 (2010).

<sup>17</sup>V. Valeau, J. Picaut, and M. Hodgson, "On the use of a diffusion equation for room-acoustic prediction," *J. Acoust. Soc. Am.* **119**, 1504–1513 (2006).

<sup>18</sup>A. Billon, V. Valeau, A. Sakout, and J. Picaut, "On the use of a diffusion model for acoustically coupled rooms," *J. Acoust. Soc. Am.* **120**, 2043–2054 (2006).

<sup>19</sup>Y. Jing and N. Xiang, "A modified diffusion equation for room-acoustic prediction (L)," *J. Acoust. Soc. Am.* **121**, 3284–3287 (2007).

<sup>20</sup>Y. Jing and N. Xiang, "On boundary conditions for the diffusion equation in room acoustic prediction: Theory, simulations, and experiments," *J. Acoust. Soc. Am.* **123**, 145–153 (2008).

<sup>21</sup>A. Billon, C. Foy, J. Picaut, V. Valeau, and A. Sakout, "Modeling the sound transmission between rooms coupled through partition walls by using a diffusion model," *J. Acoust. Soc. Am.* **123**, 4261–4271 (2008).

<sup>22</sup>N. Xiang, Y. Jing, and A. Bockman, "Investigation of acoustically coupled enclosures using a diffusion-equation model," *J. Acoust. Soc. Am.* **126**, 1187–1198 (2009).

<sup>23</sup>N. Xiang, J. Escolano, J. M. Navarro, and Y. Jing, "Investigation on the effect of aperture sizes and receiver positions in coupled rooms," *J. Acoust. Soc. Am.* **133**(6), 3975–3985 (2013).

<sup>24</sup>J. M. Navarro, J. Escolano, and J. J. Lopez, "Implementation and evaluation of a diffusion equation model based on finite difference schemes for sound field prediction in rooms," *Appl. Acoust.* **73**, 659–665 (2012).

<sup>25</sup>M. Barron, "Interpretation of early decay times in concert auditoria," *Acta Acust. Acust.* **81**, 320–331 (1995).

<sup>26</sup>E. Cirillo and F. Martellotta, "Sound propagation and energy relations in churches," *J. Acoust. Soc. Am.* **118**(1), 232–248 (2005).

<sup>27</sup>S. Chiles and M. Barron, "Sound level distribution and scatter in proportionate spaces," *J. Acoust. Soc. Am.* **116**(3), 1585–1595 (2004).

<sup>28</sup>J. S. Anderson and M. Bratos-Anderson, "Acoustic coupling effects in St. Paul's Cathedral, London," *J. Sound Vib.* **236**(2), 209–225 (2000).

<sup>29</sup>P. Luizard and B. F. G. Katz, "Coupled volume multi-slope room impulse responses: A quantitative analysis method," in *Proceedings of the Institute of Acoustics, 8th International Conference on Auditorium Acoustics*, Dublin, May 20–22, 2011, pp. 169–176.

<sup>30</sup>M. R. Schroeder, "New method of measuring reverberation time," *J. Acoust. Soc. Am.* **37**, 409–412 (1965).

<sup>31</sup>L. L. Beranek, *Concert Halls and Opera Houses: Music, Acoustics and Architecture*, 2nd ed. (Springer-Verlag, New York, 2004), 667 p.

<sup>32</sup>E. Kahle, Y. Jurkiewicz, N. Faille, T. Wulfrank, and B. F. G. Katz, "La Philharmonie de Paris concert hall competition," in *Proceedings of the International Symposium on Room Acoustics (ISRA)*, Sevilla, Spain, September 10–12, 2007.

<sup>33</sup>J. H. Rindel, "The use of computer modeling in room acoustics," *J. Vibroeng.* **3**(4), 219–224 (2000).

- <sup>34</sup>H. Pu, X. Qiu, and J. Wang, "Different sound decay patterns and energy feedback in coupled volumes," *J. Acoust. Soc. Am.* **129**(4), 1972–1980 (2011).
- <sup>35</sup>M. Barron, "Non-linear decays in simple spaces and their possible exploitation," in *Proceedings of the Institute of Acoustics, 8th International Conference on Auditorium Acoustics*, Dublin, May 20–22, 2011.
- <sup>36</sup>H. P. Seraphim, "Investigations on the difference limen of exponential decay for broadband impulse," *Acustica* **8**, 280–284 (1958).
- <sup>37</sup>M. R. Schroeder and K. H. Kuttruff, "On frequency response curves in rooms. Comparison of experimental, theoretical, and Monte Carlo results for the average frequency spacing between maxima," *J. Acoust. Soc. Am.* **34**, 76–80 (1962).
- <sup>38</sup>P. Luizard, J.-D. Polack, and B. F. G. Katz, "Auralization of coupled spaces based on a diffusion equation model," in *Proceedings of the Sound and Music Computing Conference, Stockholm, Sweden, July 30–August 3, 2013*.